Journal of Physics Research and Applications

Research Article

A SCITECHNOL JOURNAL

Fundamental Investigations of Fermi Surface and Optoelectronic Properties of Pyrochlore Oxide Superconductor (KOs2O6): GGA+U+SOC and DFT

Muhammad Irfan[1], Safdar Hussain[1], Saleem Ayaz Khan[2], Sikander Azam[3] and Souraya Goumri-Said[4]

Abstract

We employed first-principle calculations techniques to explore the optoelectronic properties of pyrochlore oxide superconductor named KOs2O6. Due to the existence of localized *f* and *d*-states in the electronic configuration of Osmium element, the spin orbit coupling and GGA+U approach were considered in computation in order to describe correctly the *d-d* coupling. KOs2O6 is a metallic and exhibit a large electrical conductivity as found from Fermi surface. The calculated optoelectronic properties have explored the real and the imaginary parts of the dielectric constant along with the other related optical properties like the refractive index, energy loss function and the absorption along with the reflectivity.

Keywords

Superconductors; Electronic structure; Optoelectronic properties; Fermi surface; FPLAPW; DFT

Introduction

Pyrochlore oxides have demonstrated several interesting phenomena, such as those explored in the metal–insulator transition. They can show colossal magneto resistance, magnetic frustration, and can behave as superconductors, as well as ferroelectrics [1]. The earliest pyrochlore oxide superconductor $Cd_2Re_2O_7$ having a Currie temperature (T_c=1.0K) was discovered in 2001 showing a predictable Bardeen–Cooper–Schrieffer (BCS-type) superconductivity [2]. Most recently, a novel family of pyrochlore oxide superconductors, AOs_2O_6, was synthesized and characterized with T_c=3.3, 6.3 and 9.6 K for of A=Cs, Rb and K, respectively [3-5]. Numerous experiments conducted on the pyrochlore oxide (KOs2O6) have reached a superconductivity behavior at maximum critical temperature (T_c). However, some reported deficiencies found in NMR experiments [6] with high coherence peak, have led to measure higher critical field H_{c2} ~38T [7]. These results were confirmed by the anisotropic constraint recorded from muon spin rotation (mSR) experiments [8]. Indeed, the investigational outcomes for changing A with Cs or Rb have shown a slight conventional appearance, while the method of superconductivity is expected to be identical for the three compounds [5,6].

The invention of superconductivity inside the b-Pyrochlores increases the complexity of the fundamental method. Whereas the process in $Cd_2Re_2O_7$, a-pyrochlore [7], is capable of understanding in the weak-coupling BCS supposition of superconductivity [8], Hiroi and collaborators have recommended from the onset that KOs2O6 is an eccentric superconductor, with the combination of arbitrary spin fluctuations [9]. Furthermore, Brühwiler and collaborators [10] recommended that $RbOs_2O_6$ possibly will be a predictable BCS-type superconductor, and modern pressure causes dimensions showed to take more support to their results [11]. We specify the closed resemblance among two compounds, it appears improbable that their superconductivity contains dissimilar foundation. Undoubtedly, a cautious learning of the electronic configuration of these materials explained on the bases of superconductivity process.

In this work, we have presented complete study of KOs2O6 solid and carried out a self-consistent ab-initio density-functional calculation of its electrical and optoelectronic, using the full-potential linearized augmented plane-wave (FLAPW) method. Our calculations are made within the generalized gradient approximation (GGA) to the E_{XC} (exchange-correlation). Due to the existence of localized *d*-states, we included the spin-orbit coupling (SOC) term and GGA+U approach in order to pronounce correctly the *d-d* coupling. We observed the dependence of total energy, volume, lattice constants, density of states and optical properties for the KOs2O6.

Computational Details

In this work, we used the full- potential linearized augmented plane waves (FPLAPW) method to investigate the physical properties of KOs2O6 with WIEN2k package [12]. The PBE_{sol} GGA (generalized gradient approximation) [13] is used for the exchange correlation prospective. R_{MT} represents the least muffin-tin radius, K_{max} is the cut off vector of the plane wave, and in the interstitial region $R_{MT}X$ K_{max}=8. The magnitude of principal vector in the charge density Fourier expansion has relation G_{max}=16 $Ry^{1/2}$ and angular momentum contains the value l_{max}=10. The core cut of energy is described by the valence and core separation, chosen as -6.0 Ry depressed by of spin- orbit interaction. When the total energy reaches to 10^{-5} Ry, so iteration was finished. The optical scheming reveals a denser k- mesh for the convergence, so a fine k-mesh 12×12×12 was selected. We treated the exchange correlation (E_{xc}) within the GGA (generalized gradient approximation) along with the effective Hubbard parameter, U=7.0 eV. Herein we also considered the spin–orbit coupling (SOC) due to the Os (Osmium) heavy metal using the variational approach [14,15]. For the ab-initio calculations the crystallographic parameters of KOs2O6 were taken from the experimental J.-I. Yamaura et al. work of the [16]. The structure of KOs2O6 crystallizes in a cubic structure with SG (space group) number 227 (Fd−3m) with lattice constant a = b = c = 10:089 (2) Å, and has 18 atoms per unit cell: two K (8b), four Os (16c), and twelve O (48f) which is demonstrated in Figure 1. The K, Os and O atoms are positioned at (fractional coordinates)

***Corresponding author:** Souraya Goumri-Said, College of Science, Physics Department, Alfaisal University, P.O. Box 50927, Riyadh, 11533, Saudi Arabia, Tel: 966-011-215-8984; E-mail: sosaid@alfaisal.edu

Sikander Azam, Department of Physics, The University of Lahore, Pakistan, Tel: (+92)3325794925; E-mail: sikander.physicst@gmail.com

Received: November 08, 2017 **Accepted:** December 13, 2017 **Published:** December 18, 2017

0.375 0.375 0.375, 0.0, 0.0, 0.0 and 0.3145(8) 0.125 0.125. Using the Murnaghan equation [17] we studied the ground states properties like lattice constant, bulk modulus and its derivative with respect to pressure by fitting total energy correspond to unit cell volume. Our calculated relaxed and optimized lattice parameters compared to experimentally deduced lattice parameters [16] are listed in Tables 1 and 2. These results agree well with the experimental data reported [16].

Results and Discussion

Electronic structure

Our investigated material has localized *d* states electrons, so the SOC (spin orbit coupling) cannot be overlooked. Therefore the electronic structure for the KOs2O6 cannot be explained by simple GGA functional. Hence GGA+U along with the SOC approach is used successfully in strong correlated systems to state appropriately the d-d coupling. The calculated energy band structure of KOs2O6 is demonstrated in Figure 2. As can be seen that band structure display no band gap at the E_F (Fermi level) that confirms the metallic behavior. Figure 3 shows the total and partial densities of states (TDOS/PDOS) for the KOs2O6 material within GGA+SOC+U (U=6.0 eV) approach in the energy range -8.0 to 8.0.0 eV. As we have included the U parameter to GGA, clearly one can observe a large splitting in Os-*d* states. By using the GGA+U+SOC, we also calculated the N_{EF} (density of electrons) at the Fermi level along with the electronic specific heat, $\gamma = \frac{1}{3}\pi N_{EF} K_\beta^2$.

As the electronic specific heat depends only on the N_{EF}, with the factor that all other terms are constant. The calculated value for the investigated material is 4.7 (mJ/moleK^2). The PDOS (partial densities of states) that are shown in Figure 3b confirmed the influence of GGA+U+SOC correlation on the Os-5d^6 states. The U (Hubbard) parameter split the Os-5d^6 states into both states i.e., in occupied and unoccupied states, as a result of E_F (Fermi level). The band, mainly the p states of O atom shows hybridization with Os atom around Fermi level (valence band). Contributions of s and p states of K at the Fermi level and in the occupied states are negligible. The lower part of the VB (valence band) between -8.0 ~ -4.0 eV is mainly due to the s and p states of O. Whereas in between -4.0 ~ Fermi level and around the it the main contributions come from the s and p states of O and Os atom along with the Os-*d* contribution. The d states of Os of and p states of O atom located between the Fermi level and -4.0 eV show a strong interaction between them. Also, we observed a robust contribution of Os-*d* and O-*p* states to DOS along the whole energy axis in the conduction band.

Fermi surfaces

To complete the explanation and elucidate the electrical as well as the optical characteristics due to the electronic configuration we have computed the Fermi surfaces (FS) for the accessible electronic orbital in KOs2O6 as displayed in Figures 4a, 4b and 4c. Furthermore, the Fermi surface is useful to get improved information of the states crossing the Fermi level. In the present material, the orbitals which are crossing the Fermi level beside the Γ–F route are 101 to 102, located in 2D Fermi surfaces and these FS contains two sheets (i.e. these sheets match to the numbers of bands cross the Fermi level in the absolute compound). Also, these FS are having an electronic sheets and set of holes. The vacant region includes holes and the shaded area is prepared up of electrons. The conductivity in the examined compounds is approximately dissimilar from each other as it is obvious commencing the FS iso-surfaces. Moreover, the color amended in FS takes place due to the alteration in electron velocity. The red and violet colors are indicated fast electrons while the slow velocities of electrons are exhibited with the residual color, owing to

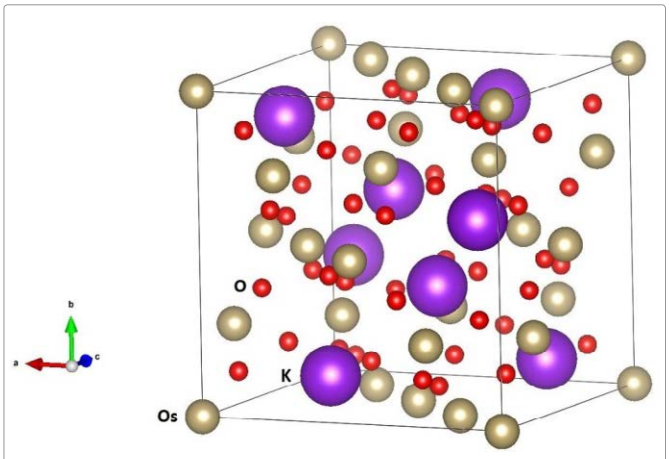

Figure 1: Unit cell structure of KOs2O6 used in the computational work.

Table 1: Comparison between experimental and optimized atomic positions for KOs2O6.

	X		Y		Z	
	Exp.	**Opt.**	**Exp.**	**Opt.**	**Exp.**	**Opt.**
K	0.375	0.391	0.375	0.391	0.375	0.391
Os	0.0	0.0	0.0	0.0	0.0	0.0
O	0.3145(8)	0.3186	0.125	0.127	0.125	0.127

Table 2: Selected bond lengths (Å) for KOs2O6 resulting from relaxation of the unit cell and compared to the experimental data [16].

Os–O (Å)		**O–Os–O (˚)**		**Os–O–Os (˚)**	
Exp.	**Opt.**	**Exp.**	**Opt.**	**Exp.**	**Opt.**
1.898(3)	1.912	90.8(3)/89.2(3)	91.05/89.9	139.9(4)	141.02

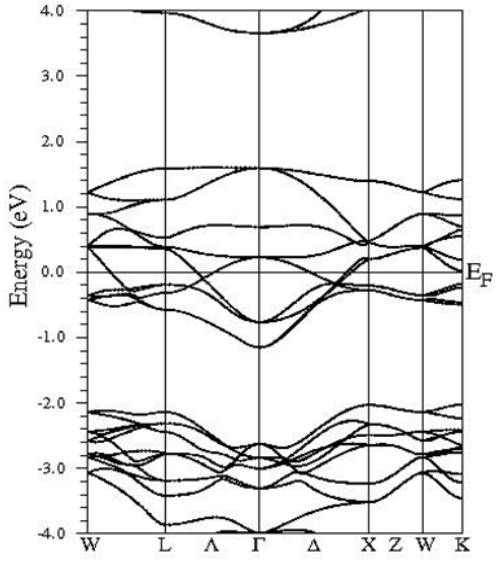

Figure 2: Energy band structure elucidating the metallic character of the pyrochlore oxide superconductor KOs2O6. The Fermi level is situated at 0.0 eV.

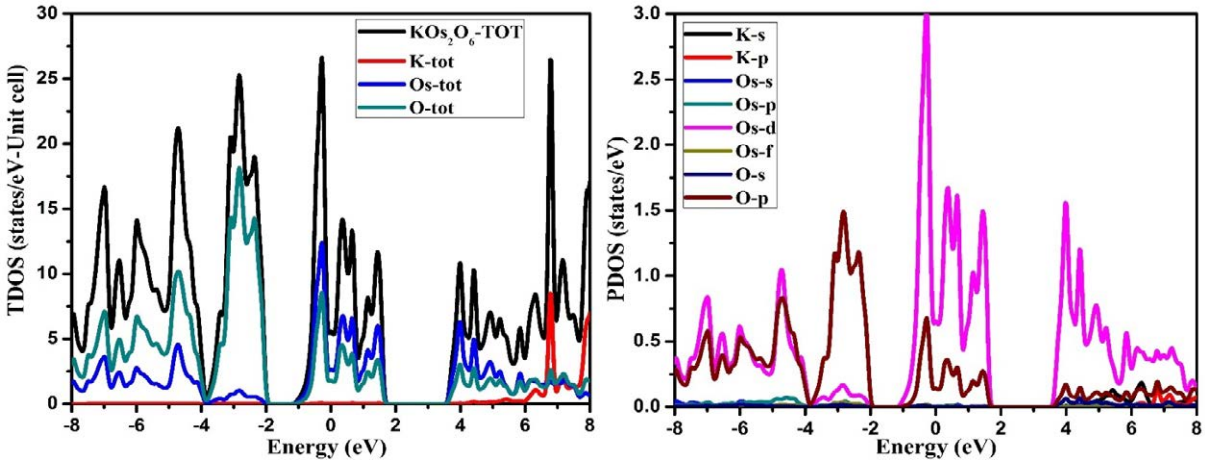

Figure 3: Total and partial densities of states. The Fermi level is situated at 0.0 e V.

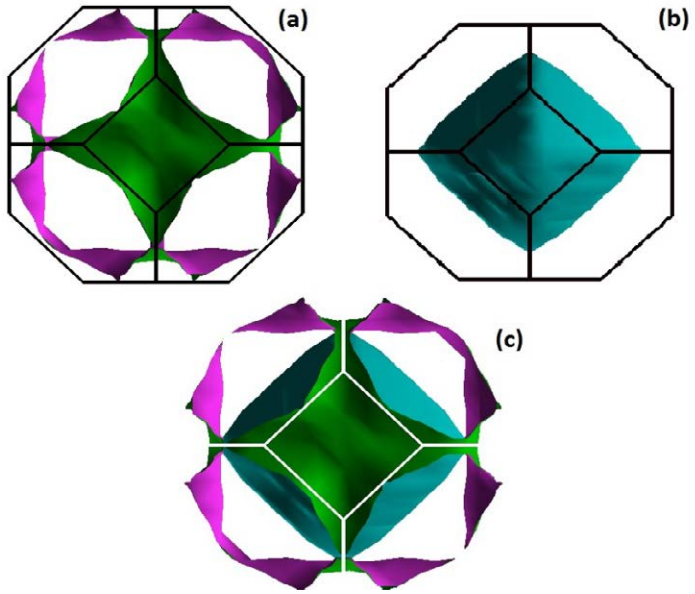

Figure 4: Fermi surface.

the intermediary velocity of electrons. It is understandable from our topological investigation of FS that the present material is showing a good electrical conductivity due its metallic character. As result, the computed FS were very helpful to investigate the job of electrons in the scheme, whose topology is immediately connected to the transport properties of materials and mostly to the electrical conductivity.

Optical properties

The optical response of the system can be investigated by dielectric constant in the presence of external electric field. The relation for dielectric constant is expressed by: $\varepsilon(\omega)=\varepsilon_1(\omega)+\varepsilon_2(\omega)$, where the real part, $\varepsilon_1(\omega)$ shows dispersive nature through the material surface and imaginary part $_2(\omega)$ illustrate light absorption of the material. In the present approximation excitonic effects are ignored but local field effect is considered. The interband and interaband transitions are contributed in $\varepsilon(\omega)$. For metals only the contribution from interaband transitions is significant. The interband transitions can further divided into direct and indirect transitions, which engage scattering of phonons and predictable to give only small contribution of$\varepsilon(\omega)$. The momentum matrix elements have been calculated on a grid of 3000 special k- points for KOs2O6. The imaginary part of dielectric function $\varepsilon_2(\omega)$ is used to analyze interband contribution by sum of all possible transitions from unoccupied and occupied states. The imaginary part can be analyzed by the formula

$$\varepsilon_2(\omega)=\frac{4\pi e^2}{m^2\omega}\int d^3k\sum_{n,n'}|<kn|P|kn'>I^2$$

$$f_{kn}(1-f_{kn'}\delta(E_{kn}-E_{kn'}-\hbar\omega)) \quad (2)$$

Where m is mass, e is electron charge, ω is the volume, $h\omega$ the energy of incident phonon, P is momentum operator, $f_{kn/}$ is the Fermi distribution, and $|kn\rangle$ represents crystal wave function. The matrix element can be evaluated from Eq. 1 by MT and interstitial regions separately. More details about the calculation matrix element s are

given elsewhere [18]. The summary over the BZ in Eq.1 is performed by linear interpolation on a network of uniformly disseminated points, the tetrahedron method [19]. The imaginary part of dielectric function $_2(\omega)$ is analyzed in the irreducible part of the BZ. The dielectric function is a tensor, and computation of all components is complex one. So we must initiate correct symmetry of the crystal to decrease the number of components. For cubic structure, we require to compute xx=yy=zz component of total dielectric function. For KOs2O6 structure [α=β=γ=90°], the dielectric tensor is then

$$\begin{pmatrix} Im\varepsilon_{xx} & 0 & 0 \\ 0 & Im\varepsilon_{xx}0 & 0 \\ 0 & 0 & Im\varepsilon_{xx} \end{pmatrix}$$

Hence, we get dielectric functions resolved into one Cartesian component. Moreover this decomposition remains valid for all optical constants given afterward. The real part of complex dielectric function is computed by Kramer-kroning relation, while imaginary part is calculated by addition of all allowed intensities in occupied and unoccupied states. If we have complex dielectric function we can compute some other parameters like absorption coefficient, refractive index, reflectivity and extinction coefficient etc.

$$\varepsilon_1(\omega) = 1+\frac{2}{\pi}M\int_0^{\infty}\frac{\omega'\varepsilon_2(\omega')}{\omega'^2-\omega^2}d\omega'$$

Where M is represents the principle value of the integral.

The optical constants i.e. refractive index $n(\omega)$, and extinction coefficient $K(\omega)$, are observed from the real and imaginary parts of the complex dielectric function as [20,21]

$$n=\left(\frac{\varepsilon_1+\left(\varepsilon_1^2+\varepsilon_2^2\right)^{\frac{1}{2}}}{\sqrt{2}}\right)^{\frac{1}{2}} \quad (3)$$

$$k=\left(\frac{-\varepsilon_1+\left(\varepsilon_1^2+\varepsilon_2^2\right)^{\frac{1}{2}}}{\sqrt{2}}\right)^{\frac{1}{2}} \quad (4)$$

Moreover, the other optical parameters, such as absorption coefficient $I(\omega)$, reflectivity $R(\omega)$, and energy loss function $L(\omega)$ are derived from $\varepsilon_1(\omega)$ and $\varepsilon_2(\omega)$ [22]. For the optical properties of KOs2O6, we select a fine k- mesh (extra k points than selected for SCF cycle). In this work, we have found good quality results for 690 k-points in IBZ, which resulted from 3000 k- points in BZ. The optical structure of KOs2O6 observed accurately by applying GGA+U+SOC functional on k- points of 12×12×12 order. Figures 5 and 6(a-e) indicate the plots of energy range [0-14] eV, of the real and imaginary parts of $\varepsilon(\omega)$and related optical properties respectively. It is observed from the calculated spectra of $\varepsilon_1(\omega)$ that the zero frequency $\varepsilon_1(0)$ depends upon energy band gap. As the under investigated material has the metallic nature so the absorption starts from 0.0 eV and its value of $\varepsilon_1(0)$ = 76.0. After that it reduces and goes to negative around 1.0 eV and attain the zero value above 2.0 eV. The value of $\varepsilon_1(\omega)$ is negative in between 1.0 – 2.6 eV. The negative value of $\varepsilon_1(\omega)$ reveals that incident light is reflected totally from the surface of material, which shows the metallic nature of the samples. The main parameter for the design of optoelectronic devices is imaginary part of dielectric function. The energy band gap and maximum absorption intensity of light in a specific region can be computed by using $\varepsilon_2(\omega)$. The maximum value of $\varepsilon_2(\omega)$ arise at energy less than 0.5 eV. After this it decreases and finally reaches the zero. The refractive index and extinction coefficient are calculated from the following relations $\varepsilon_1(\omega)= n^2-k^2$ and $\varepsilon_2(\omega)= 2nk$. Figure 6a, represents the graphical analysis of the $n(\omega)$, $k(\omega)$, where they exhibit the same behavior as the dielectric constants $\varepsilon_1(\omega)$,$\varepsilon_2(\omega)$. Moreover, $n(0)$ and $\varepsilon_1(0)$ satisfy the relation $n_0^2 = \varepsilon_1(0)$ and agreed well with our optimized result. In addition $n(\omega)$is dimensionless and shows the propagation of energy in the matter. $n(\omega)$ varies with wavelength of light due to dispersion, from which light splits its constituent colours. The value of $n(\omega)$, must be higher in the optical field and most of the materials have in the range of one and two. In our observation, the maximum value of $n(\omega)$ for is > 0.5 eV. The peaks of plot disappear at the higher energy. It means that transparency of materials decreases at higher energy, and due to band transition (valence to conduction) high energy photons are absorbed. The value of $n(\omega)$ less than unity in the region 10-14 eV. Moreover, it is observed from the fractional refractive index that the group velocity is higher than speed of light, and this velocity shifts to negative values. This behavior might lead to consider the present material for non-linear response. For the surface analysis of the samples reflectivity (Figure 6b) is also computed, which is the difference of the incident and reflected power as describe in the Figure 6a, its value at zero frequency limit R(0) is 64 %. The peaks of $R(\omega)$ is analogous to the peaks $\varepsilon_1(\omega)$. So the value reflectivity $R(\omega)$ is maximum in the region where absorption coefficient covers minimum value. Furthermore, there are large numbers of peaks laying in the spectrum region lower energy range. It is more surprising that maximum value of $R(\omega)$ and minimum value of $\varepsilon_1(\omega)$ investigated in the same region. This is due to fact, that in the metallic portion all incident radiations are reflected and the band gap is zero, lacking absorption of incident light. In the inset of Figure 6d, we can see that at the point where we have increase in the reflectivity we have at that point we have decrease in the energy loss function (see Fig 6c). $k(\omega)$ and $\varepsilon_2(\omega)$ have same nature, and are very useful to find the absorption of light and band edge by using the relation $\alpha=\frac{4\pi k}{\lambda}$. The peaks of $k(\omega)$ and $n(\omega)$ are showing tendency from valence to conduction band, which occur due to a direct transition. The α (absorption coefficient) is very prominent parameter, used to approximate the

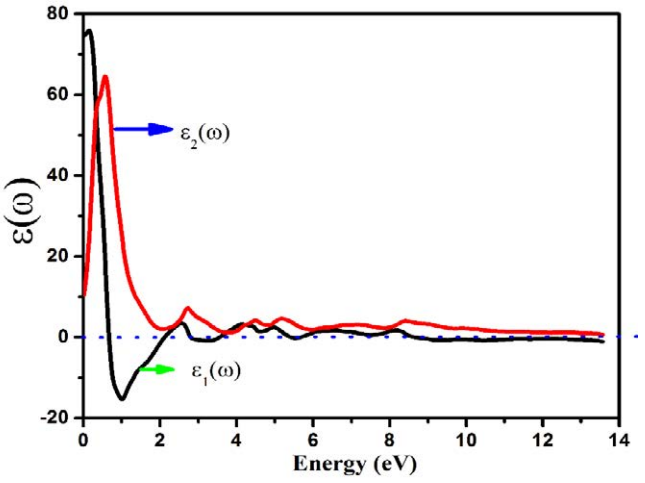

Figure 5: Imaginary and real parts of the dielectric function.

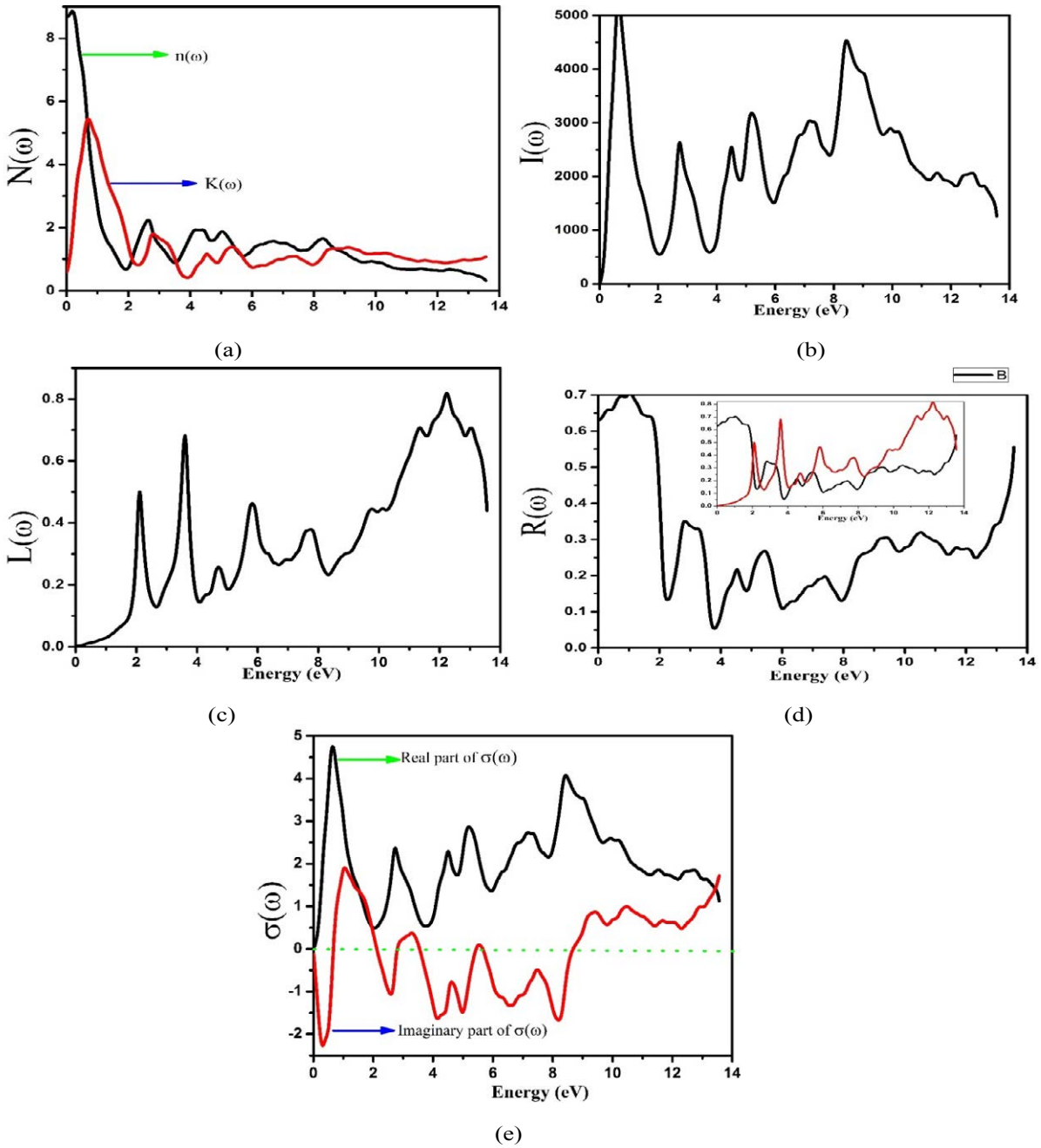

Figure 6: The extracted related optical properties from electronic structure : (a) refractive index, (b) extinction coefficient, (c) energy loss function, (d) reflectivity and (e) conductivity.

decaying rate of intensity per unit band gap and distance of the investigating material. The maximum value of α lies in the selected energy range between 0.0 ~ 14.0 eV, which is shown in the inset of Figure 6d. Figure 6e shows the optical conductivity $\sigma(\omega)$for KOs2O6. As we are dealing with a metallic material so the absorption starts from 0.0 eV. From the plots it is shown that $\sigma(\omega)$ reaches its highest values in 0.5 ~ 10.0 eV ranges and then drops to smallest amount with supplementary growth in the photon energy. Consequently it is analyzed that all peaks, particulars of $\sigma(\omega)$coincide with the peaks of α for both compounds, in the deliberated range of energy. So the $\sigma(\omega)$ occurs in these compounds due to the absorption in the first BZ one beside high symmetry points.

Conclusion

We employed the first-principle approach that is based on the DFT (density functional theory) method with GGA+U+SOC (spin-orbit coupling), to explore the electronic and optoelectronic properties of pyrochlore oxide superconductor KOs2O6. The ground state properties that are based on the internal structure parameters, like lattice constants and bulk modulus were comprehended from the structural relaxation and optimization. The employed

computational approach (i.e., GGA+U+SOC) produced a correct description of the structural parameters along with the electronic properties. We have also studied the Fermi surface shape to assess their behaviors. We also focused on the optoelectronic properties in which we studied the dielectric function like the real and the imaginary parts along with the other related optical properties. As KOs2O6 has a metallic nature therefore the inter-band and intra-band transitions are contributed in $\varepsilon(\omega)$. For metals only the contribution from intra-band transitions is significant. There have been no previous experimental or theoretical results for the electronic optical properties available for the present pyrochlore oxide superconductor KOs2O6. These outcomes of the current study can be considered as a prediction study with the hope that it will stimulate other research on these materials.

References

1. Subramanian MA, Aravamudan G, Rao GVS (1983) Oxide pyrochlores- A review. Prog Solid State Chem 15: 55-143.
2. Hanawa M, Muraoka Y, Tayama T, Sakakibara T, Yamaura J, et al. (2001) Superconductivity at 1 K in $Cd_2Re_2O_7$. Phys Rev Lett 87: 187001.
3. Yonezawa S, Muraoka Y, Matsushita Y, Hiroi Z (2004) Superconductivity in a pyrochlore-related oxide KOs2O6. J Phys Condens Matter 16: L9-L12.
4. Yonezawa S, Muraoka Y, Matsushita Y, Hiroi Z (2004) New Pyrochlore Oxide Superconductor $RbOs_2O_6$. J Phys Soc Jpn 73: 819-821.
5. Yonezawa S, Muraoka Y, Hiroi Z (2004) New β-Pyrochlore Oxide Superconductor $CsOs_2O_6$. J Phys Soc Jpn 73: 1655-1656.
6. Brühwiler M, Kazakov SM, Zhigadlo ND, Karpinski J, Batlogg B (2004) Superconductivity in the geometrically frustrated pyrochlore $RbOs_2O_6$. Phys Rev B 70: 020503.
7. Hanawa M, Muraoka Y, Tayama T, Sakakibara T, Yamaura J, Hiroi Z (2001) Superconductivity at 1 K in $Cd_2Re_2O_7$. Phys Rev Lett 87: 187001.
8. Hiroi Z, Yonezawa S, Muraoka Y (2004) Unprecedented Superconductivity in β-Pyrochlore Osmate KOs2O6. J Phys Soc Jpn 73: 1651-1654.
9. Koda A, Higemoto W, Ohishi K, Saha SR, Kadono R, et al. (2005) Possible Anisotropic Order Parameter in Pyrochlore Superconductor KOs2O6 Probed by Muon Spin Rotation. J Phys Soc Jpn 74: 1678-1681.
10. Yonezawa S, Muraoka Y and Hiroi Z (2004) New β-Pyrochlore Oxide Superconductor $CsOs_2O_6$. J Phys Soc Jpn 73: 1655-1656.
11. Hiroi Z, Hanawa M (2002) Superconducting properties of the pyrochlore oxide $Cd_2Re_2O_7$. J Phys Chem Solids 63: 1021-1026.
12. Blaha P, Schwarz K, Madsen GKH, Kvasnicka D, J Luitz (2001) WIEN2K, An augmented plane wave + local orbitals program for calculating crystal properties. Thesis, Technische Universität Wien, Austria.
13. Perdew JP, Ruzsinszky A, Csonka GI, Vydrov OA, Scuseria GE, et al. (2008) Restoring the Density-Gradient Expansion for Exchange in Solids and Surfaces. Phys Rev Lett 100:136406.
14. Bendjedid A, Seddik T, Khenata R, Baltache H, Murtaza G, et al. (2015) GGA+U study on phase transition, optoelectronic and magnetic properties of AmO_2 with spin–orbit coupling. J Magn Magn Mater 396: 190-197.
15. Azam S, Khan SA, Minar J, Khan W, Din H, et al. (2015) Coulomb interaction and spin-orbit coupling calculations of thermoelectric properties of the quaternary chalcogenides Tl_2PbXY_4 (X = Zr, Hf and Y = S, Se). Semicond Sci Technol 30: 105018.
16. Yamaura J, Yonezawa S, Muraoka Y, Hiroi Z, et al. (2006) Crystal structure of the pyrochlore oxide superconductor KOs2O6. J Solid State Chem 179 336-340.
17. Murnaghan FD (1944) The Compressibility of Media under Extreme Pressures. Proc Natl Acad Sci U S A 30: 244-249.
18. Ambrosh-Draxl C, Sofo JO (2006) Linear optical properties of solids within the full-potential linearized augmented planewave method. Comput Phys Commun 175: 1-14.
19. Blochl PE, Jepsen O, Andersen OK (1994) Improved tetrahedron method for Brillouin-zone integrations. Phys Rev B 49:16223.
20. Delin A, Eriksson AO, Ahuja R, Johansson B, Brooks MS, et al. (1996) Optical properties of the group-IVB refractory metal compounds. Phys Rev B 54: 1673.
21. Amin B, Ahmad I, Maqbool M, Goumri-Said S, Ahmad R (2011) Ab initio study of the bandgap engineering of Al1−xGaxNAl1−xGaxN for optoelectronic applications. J Appl Phys 109: 023109.
22. Saha S, Sinha TP, Mookerjee A (2000) Electronic structure, chemical bonding, and optical properties of paraelectric $BaTiO_3$. Phys Rev B 62: 8828.

Author Affiliation

Top

[1]*Department of Physics, University of Sargodha, 40100 Sargodha, Pakistan*

[2]*New Technologies e Research Center, University of West Bohemia, Univerzitni 8, 306 14 Pilsen, Czech Republic*

[3]*Department of Physics, the University of Lahore, 40100 Sargodha, Pakistan*

[4]*College of Science, Physics Department, Alfaisal University, P.O. Box 50927, Riyadh, 11533, Saudi Arabia*